Influence of Fe and Si on the microstructure of the Al-Mn alloy with Zr addition

M. Karlík[1]*, M. Slámová[2†], T. Mánik[1]

[1] *Czech Technical University in Prague, Faculty of Nuclear Sciences and Physical Engineering, Department of Materials, Trojanova 13, 120 00 Prague 2, Czech Republic*
[2] *Research Institute for Metals Inc., Panenské Břežany, 250 70 Odolena Voda, Czech Republic*

Received 26 February 2009, received in revised form 17 March 2009, accepted 17 March 2009

Abstract

The aim of experimental part was to study the influence of Si and Fe on precipitation, recrystallization response, size and formation of secondary phases in the alloys. The hardness and electrical conductivity measurements and light metallography observations were carried out after one- and two-step precipitation annealing. The density of precipitates in all alloys was lower and the primary phases were much coarser in the surface regions of the 2 mm sheets than in the middle. The differences in hardness, electrical conductivity and the microstructure between one- and two-step annealing were only very small. But the two-step precipitation annealing procedure led to the same or lower decrease of the particle density during annealing. Small equiaxial grains were formed in the alloys with Si addition. Except Al-Mn-Zr, the alloys without Si (Al-Mn and Al-Mn-Zr-Fe) showed long recrystallized grains in the surface regions of the sheets. Only the Al-Mn-Zr alloy showed a cold-worked microstructure in the whole cross section of the sheet after the entire one- or two-step annealing procedures. Therefore, Si and/or Fe additions degrade the recrystallization resistance of the Al-Mn alloy with Zr addition and their amount in the commercial alloys should be reduced.

K e y w o r d s: aluminium alloys, microstructure, precipitation, resistance to recrystallization, microhardness test, electrical conductivity

1. Introduction

Following a strong demand for weight reduction of automotive heat exchangers, research and development effort is devoted to reduce the thickness of aluminium alloy fin stock below 0.1 mm. The mechanical strength of the fin has to be high to avoid buckling [1], and at the same time the alloy should be recrystallization resistant to keep its strength after brazing. In order to obtain a good recrystallization resistance, the alloy should contain a dense and homogeneous distribution of second phase particles.

The best way to achieve this microstructure in Al alloys is to add a small amount (0.2–0.3 wt.%) of Sc leading to the formation of Al_3Sc dispersoids [2]). Unfortunately, scandium is extremely expensive and its application in aluminium alloys for automotive industry is not possible. A similar effect can also be obtained by Zr addition (0.5–0.8 wt.%), resulting in the formation of the Al_3Zr phase [3–6], having either metastable ($L1_2$) or stable ($D0_{23}$) crystal structure, depending on the thermal history of the alloy (heating/cooling rate during casting, homogenization procedure, etc.) [7–9].

Silicon and iron, always present in the commercial alloys, have a substantial effect on the phase composition of Al-Mn alloys. In the pure Al-Mn binary alloys, the decomposition of the supersaturated solid solution is very sluggish [10, 11]. Additions of Fe and Si greatly decrease the solubility of Mn in solid solution and accelerate the precipitation rate of secondary Mn-bearing phases, i.e. Al_6Mn or $Al_6(Fe,Mn)$, and $Al_{15}Mn_2Si_3$ or α-$Al_{12}(Mn,Fe)_3Si$ [10–14]. Moreover, in Zr-containing alloys Fe and Si increase the rate of formation of Al_3Zr particles, acting as catalysts. The Al_3Zr dispersoids precipitate usually on the Si and

*Corresponding author: tel.: +420 224 358 507; fax: +420 224 358 532; e-mail address: Miroslav.Karlik@fjfi.cvut.cz

Fe atom clusters [3]. Furthermore, Si has also a positive effect on Al_3Zr stability. The $D0_{22}$ compound $(Al_{0.72}Si_{0.28})_3Zr$ with Si atoms in its Al sublattice is more stable than $D0_{23}$ or $L1_2$ crystal structures [15].

One of the main problems of using Al_3Zr in order to inhibit recrystallization is that these dispersoids are usually heterogeneously distributed, due to the microsegregation of Zr and its low diffusivity [5]. A more homogeneous distribution of Al_3Zr particles can be achieved by a two-step precipitation annealing [4, 16]. The purpose of the present paper is to study the influence of Si, Fe, and both these elements on the microstructure and properties of Al-Mn-Zr alloy subjected to one-step and two-step precipitation annealing.

2. Experimental details

The experimental alloys were produced using an Al-1.43wt.%Mn base alloy by direct-chill (DC) casting to billets of the dimensions of 20 mm × 55 mm × 100 mm. The results of the chemical analysis are given in Table 1. After scalping, the billets were cold rolled with 89 % reduction (the equivalent strain $\varepsilon \sim 2.5$) to the thickness of 2 mm. One-step and two-step annealing were applied after cold rolling in order to compare the final microstructure, particularly the homogeneity of the distribution and the density of secondary phase particles. Heating to 450 ℃, soaking for 12 hours at this temperature, and cooling (50 ℃ h^{-1}) were applied during one-step annealing. The two-step annealing involved holding the samples for 10 hours at the temperature of 250 ℃, heating to 450 ℃ and soaking for 12 hours followed by cooling down at the same rate as in the case of one-step annealing. The scheme of both annealing procedures is in Fig. 1.

Vickers hardness measurements with 10 kg load (HV 10) were carried out in order to determine approximately the onset and the progress of the softening processes, recovery and recrystallization. The precipitation reactions during annealing and the changes in the solid solution concentrations were monitored by electrical conductivity measurements performed using the Forster Sigmatest device. The microstructure of the samples was studied by Nikon Epiphot 300 metallographic microscope equipped with the camera Hitachi-HBC 20A. The examined stages during annealing (designed by $Z = 0$–8) are shown in Fig. 1. The second phase particles were revealed using a 0.5 % solution of hydrofluoric acid in water. The grain structure was visualized in the polarized light after anodizing in the Barker's reagent. The precipitate size and density were determined using the Image Processing toolkit in the Matlab® software, after pre-processing (normalizing) of the images to gain the same brightness representation of the identical image elements (precipitates) as well as the background in the whole image series.

Table 1. Chemical composition of studied alloys (wt.%)

Alloy	Mn	Zr	Si	Fe	Al
Al-Mn	1.52	0.0	0.05	0.01	balance
Al-Mn-Zr	1.39	0.1	0.08	0.01	balance
Al-Mn-Zr-Fe	1.44	0.1	0.06	0.22	balance
Al-Mn-Zr-Si	1.43	0.1	0.21	0.01	balance
Al-Mn-Zr-Si-Fe	1.46	0.1	0.23	0.22	balance

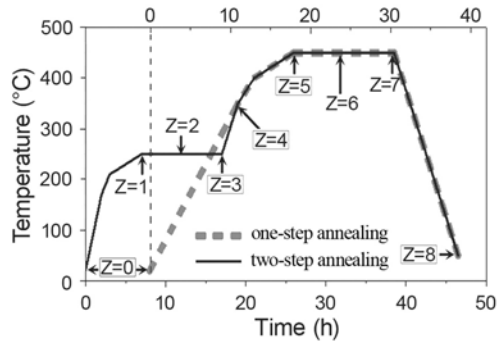

Fig. 1. Scheme of one- and two-step annealing. Since both curves are overlaying at the final part of process, the x-axis for one-step annealing is shifted. The hardness measurement was carried out in the stages $Z = 0$–8 and light microscopy was performed in the stages marked in the boxes.

3. Results

3.1. Cast microstructure

As expected, all alloys showed a similar, coarse grain structure after casting. The differences in the alloy composition influenced the primary phase formation. Almost no coarse primary phases were found in Al-Mn and Al-Mn-Zr alloys. Only a low fraction of $Al_{15}Mn_2Si_3$ primary phase was present in the Al-Mn-Zr-Si alloy (Fig. 2a), while the alloys containing Fe showed a distinct amount of $Al_6(Mn,Fe)$ and α-$Al_{12}(Mn,Fe)_3Si$ primary phases (Fig. 2b,c) which appeared on the dendrite boundaries inside the grains. The dendrite arm spacing ranged from 100 to 300 μm (Fig. 2c), elongated dendrites were frequently more than 1 mm long (Fig. 2b).

3.2. Hardness and electrical conductivity

On the sheets cold rolled to 2 mm, hardness and electrical conductivity were measured in the initial condition ($Z = 0$ in Fig. 1), and on other samples

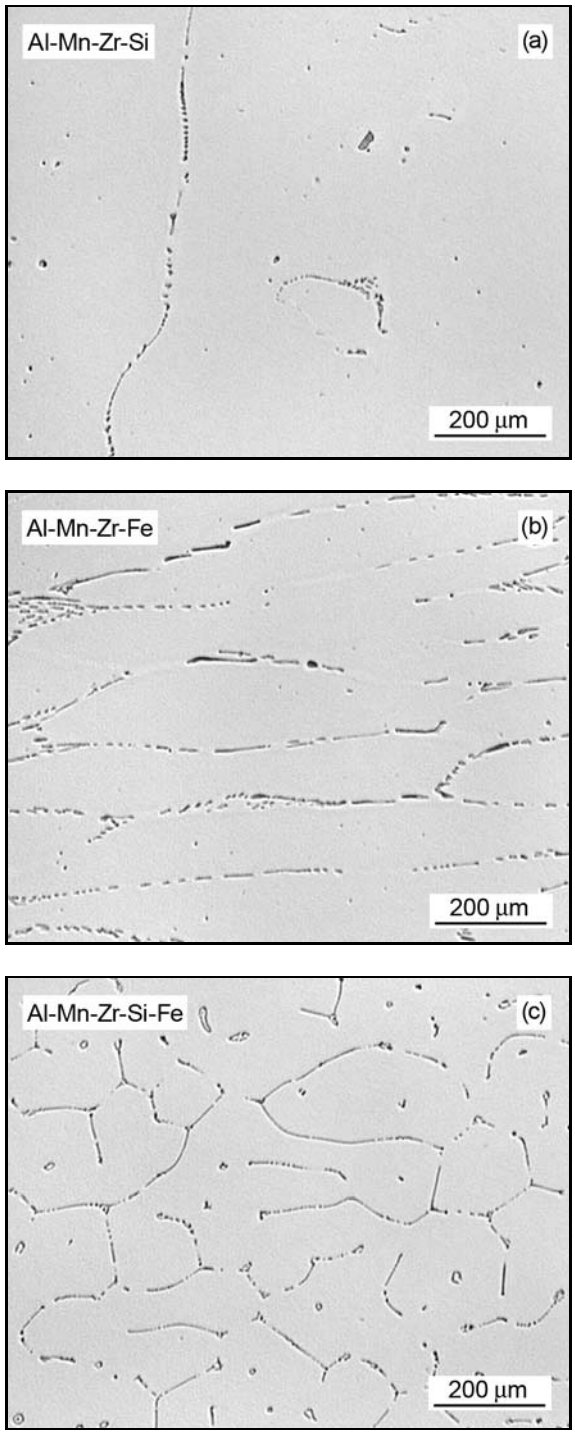

Fig. 2. Microstructure of alloys Al-Mn-Zr-Si (a), Al-Mn--Zr-Fe (b), and Al-Mn-Zr-Si-Fe (c) after casting. The micrographs of Al-Mn and Al-Mn-Zr alloys are not presented here because they exhibited only a low amount of coarse primary phases (for Al-Mn-Zr alloy see also Fig. 6).

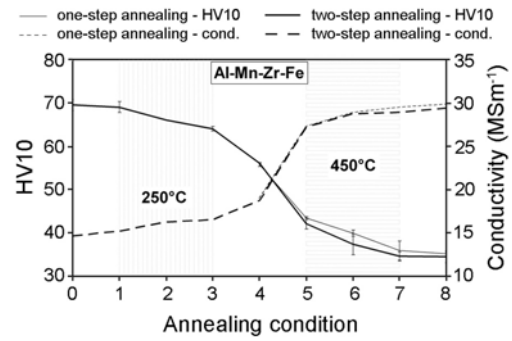

Fig. 3. The evolution of hardness and electrical conductivity of the Al-Mn-Zr-Fe alloy subjected to one- and two-step annealing, as a function of the annealing condition Z designed in Fig. 1. (This alloy showed the most important differences of the values in the annealing conditions 5 to 8.)

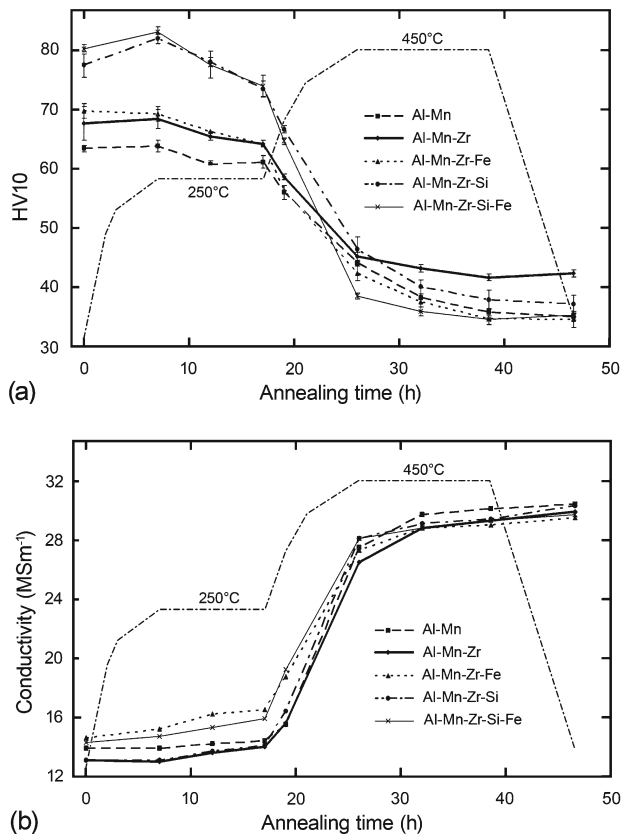

Fig. 4. The evolution of hardness (a) and electrical conductivity (b) of all alloys subjected to a two-step annealing procedure. For the sake of clarity, the corresponding temperature course is also plotted.

taken at different points of the annealing curve. In the case of one- and two-step annealing the selected conditions were $Z = 4$–8, and $Z = 1$–8, respectively (Fig. 1). The differences between the hardness and the conductivity of the samples subjected to one- and two-step annealing were thus expected in the corresponding points 4–8. Surprisingly, these differences were only very small, as it is illustrated in Fig. 3 for the Al-Mn-Zr-Fe alloy that exhibited the highest vari-

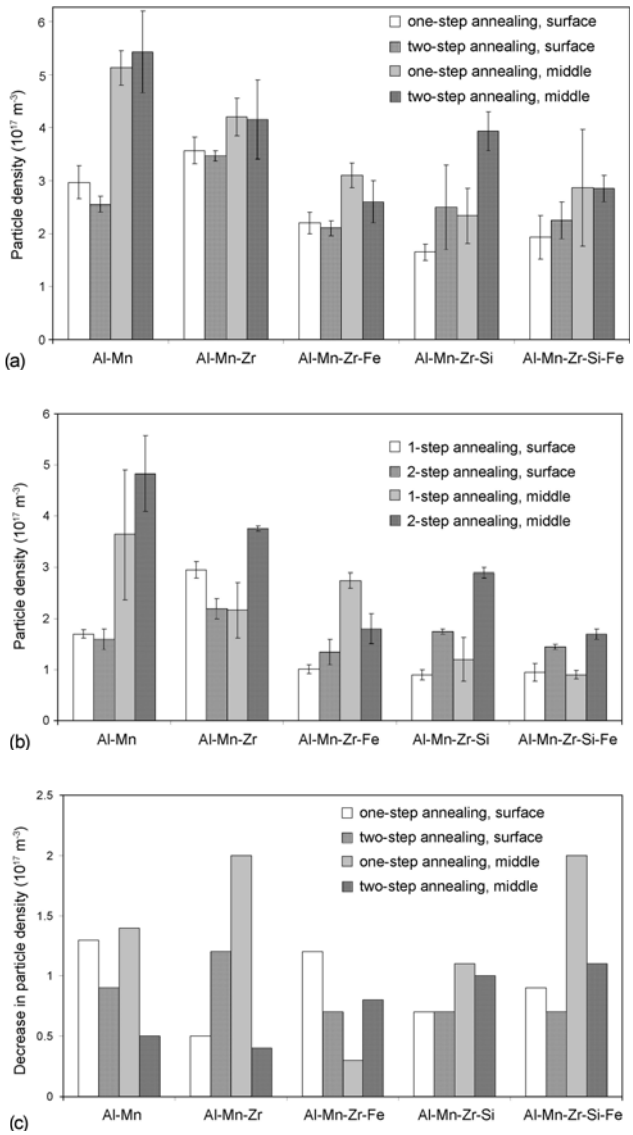

Fig. 5. Number density of the precipitates close to the surface and in the middle of the sheets for both one- and two-step annealing procedures: (a) at the onset of the soaking period ($Z = 5$), (b) after cooling ($Z = 8$), (c) the corresponding decrease of the particle density (values at $Z = 8$ subtracted from the values at $Z = 5$).

ances of the values. From Fig. 3 it follows that the two-step annealing leads to somewhat lower hardness and conductivity of the Al-Mn-Zr-Fe alloy, but the differences are only within the range of the experimental scatter. For other four alloys, these differences were even lower. In consequence, only the results obtained after two-step annealing are presented in some figures below.

The evolution of hardness and electrical conductivity of all five alloys as a function of time during two-step annealing procedure is in Fig. 4. For the sake of clarity, the corresponding temperature course is also plotted. For all five alloys, the most important drop of hardness accompanied by a steep increase of electrical conductivity arises during heating up from 250 to 450 °C. In this period, most of the precipitates are formed, and the solid solution depletes of the solute atoms. In the following 12 h soaking period, the conductivity slightly increases and the hardness somewhat decreases. If we compare the values in the initial condition ($Z = 0$), the hardness values are in the order of the amount of alloying elements in the solid solution, i.e., the lowest hardness has the binary alloy Al-Mn (63 HV 10), followed by the ternary one Al-Mn-Zr (67 HV 10), quaternary Al-Mn-Zr-Fe (69 HV 10), Al-Mn-Zr-Si (78 HV 10), and finally Al-Mn-Zr-Si-Fe (80 HV 10) (see also Table 1). If we take into account only the quaternary alloys, the hardening effect of Si in the solid solution is higher than that of Fe, as expected, because of higher Si solubility. Throughout annealing at 250 °C, the hardness decreases due to recovery; the important drop of hardness in the middle of the annealing period is due to recrystallization. In the final annealing condition ($Z = 8$), the hardness of the Al-Mn, Al-Mn-Zr-Fe, and Al-Mn-Zr-Fe-Si is comparable (34 HV 10), while the Al-Mn-Zr-Si alloy shows only a small increase (36 HV 10) indicating that silicon has a small positive effect on precipitate formation. The highest hardness values not only in the final condition (42 HV 10), but also during the whole soaking period, were measured for the Al-Mn-Zr alloy (Fig. 4a). As for the values of the conductivity, the differences between individual alloys are not so important. The values range from 13 to 14 MS m^{-1}, and from 29 to 30.5 MS m^{-1} in the initial and final condition, respectively. More important differences are only in the middle of the annealing period (Fig. 4b), where the secondary particles precipitate.

3.3. Secondary phase formation

The size and the distribution of the particles were examined by light microscopy in the stages $Z = 0$, 3, 4, 5, and 8 (Fig. 1). A quantitative comparison of the particle density at the surface and in the middle region of the cross section of the sheets of all five alloys was carried out in the beginning of the soaking period ($Z = 5$, Fig. 5a), and in the final condition ($Z = 8$, Fig. 5b). Figure 5 involves the results for both one- and two-step annealing procedures. From the graphs in Fig. 5a,b it can be concluded that the density of the particles decreases with the amount of alloying elements. In other words, the addition of Fe, Si or both of these elements has a negative effect on the precipitation of fine particles. If we compare the graphs (a) and (b), representing respectively the onset of the soaking period ($Z = 5$) and the final condition ($Z = 8$), it is obvious that the density of the particles of all five alloys decreases due to their dissolution and coarsening during annealing at 450 °C and cooling. Another com-

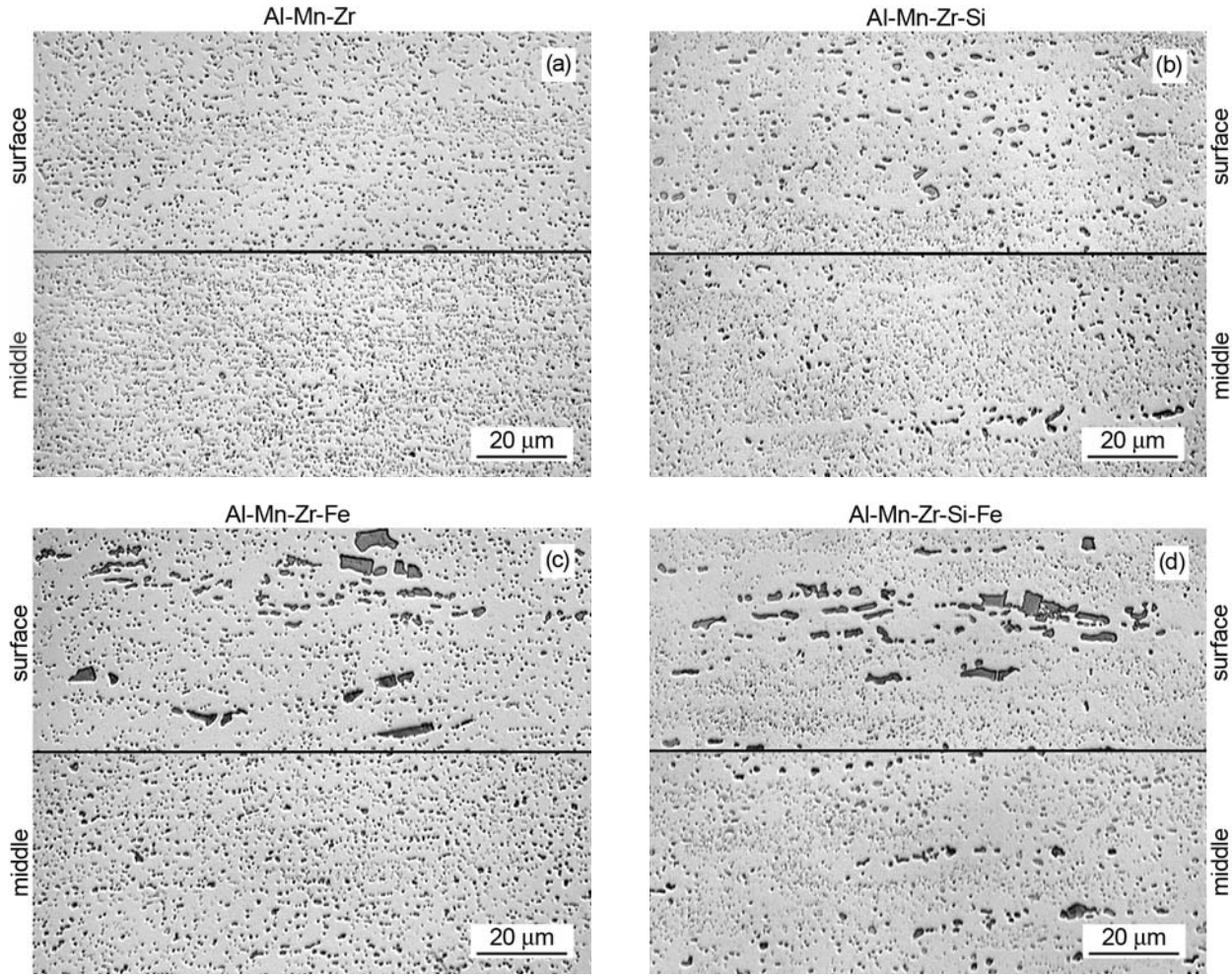

Fig. 6. Micrographs of the particles in Al-Mn-Zr, Al-Mn-Zr-Si, Al-Mn-Zr-Fe, and Al-Mn-Zr-Si-Fe alloys taken close to the surface and in the middle regions of the 2 mm sheet subjected to the whole two-step annealing procedure ($Z = 8$). The micrographs of the binary alloy were almost the same as for the Al-Mn-Zr alloy.

parison is possible between the one- and two-step annealing. It follows that the two-step annealing yields a comparable density of the particles at the surface and mostly higher in the middle of the sheets. The beneficial effect of the two-step annealing procedure is better seen in Fig. 5c showing the corresponding decrease of the particle density – values at $Z = 8$ (Fig. 5b) subtracted from the values at $Z = 5$ (Fig. 5a). Except for the Al-Mn-Zr alloy on the surface and the Al-Mn-Zr--Fe alloy in the middle, the two-step annealing leads to the same or lower decrease of the particle density during annealing.

The micrographs of the particles, corresponding to the final condition after two-step annealing and cooling ($Z = 8$) of the Al-Mn-Zr, Al-Mn-Zr-Fe, Al-Mn-Zr--Si, and Al-Mn-Zr-Si-Fe alloys are presented in Fig. 6. The binary alloy is not included since its micrographs were almost the same as those of the Al-Mn-Zr alloy. To give a true picture of the differences in the microstructure, each part of the figure is combined from two micrographs recorded close to the surface and in the middle of the 2 mm sheets. At the first view it is obvious that the density of the particles close to the surface is lower than in the middle of the sheets. The Al--Mn-Zr alloy (Fig. 6a) shows a homogeneous distribution of fine particles through the whole cross section of the sheet; however the particles are somewhat coarser at the surface. The addition of Si (Fig. 6b) leads to distinctly coarser particles having a less homogeneous distribution. In the middle of the sheet there are bands without fine precipitates along coarser particles. The alloy with Fe addition (Fig. 6c) shows coarse primary phases namely close to the surface of the sheet. In the vicinity of these coarse particles, fine secondary precipitate is often absent. Furthermore, the fine secondary particles in the middle of the sheet are distinctly coarser than in the case of the Al-Mn-Zr alloy. The addition of Si and Fe (Fig. 6d) leads to coarse primary phase formation and also to the coarsening of the secondary precipitate. Depleted regions, where fine secondary particles are absent, can be seen not only along the primary phases, but also in other regions at the

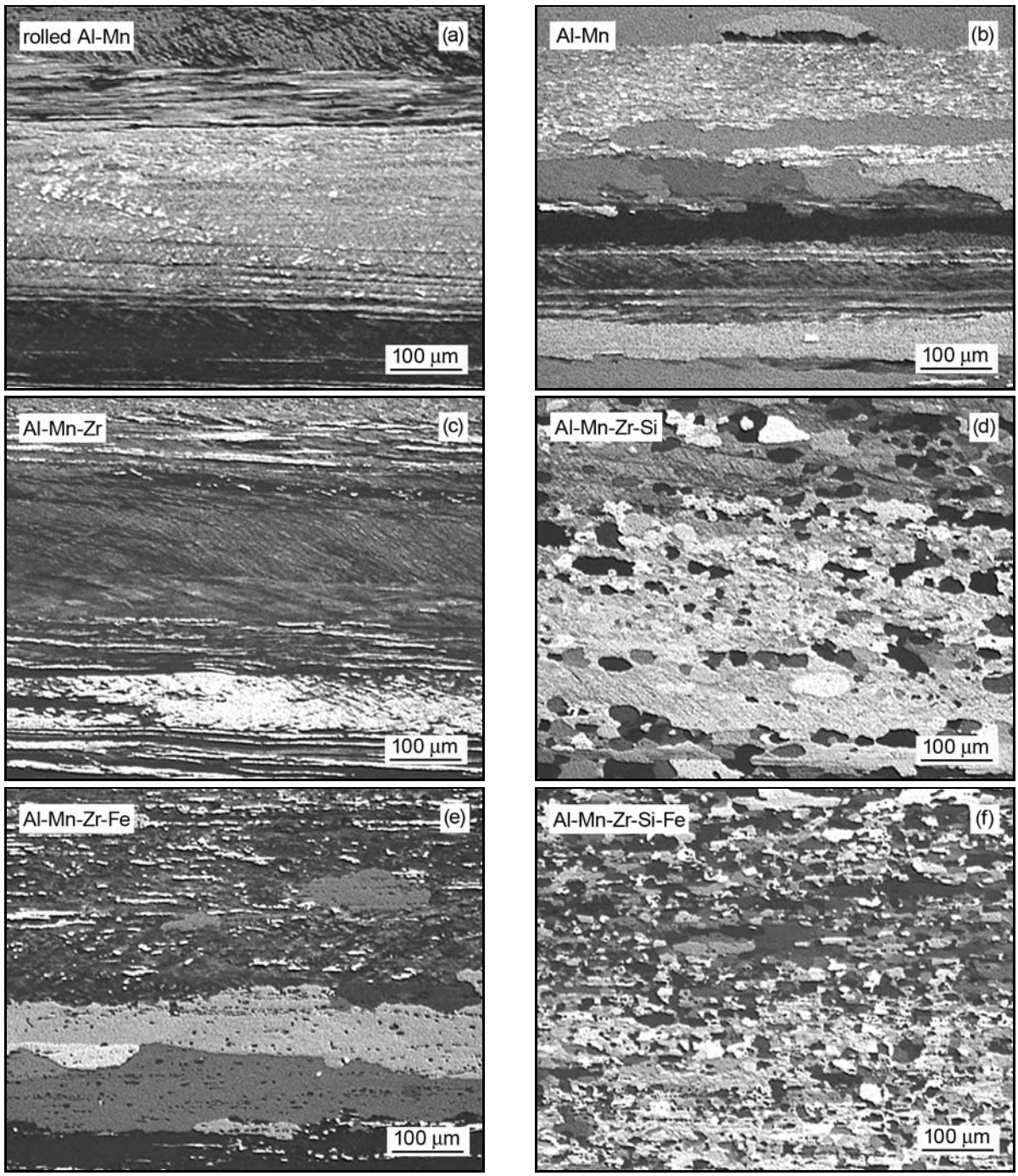

Fig. 7. Grain structure close to the surface of the sheet: (a) rolled Al-Mn alloy ($Z = 0$), (b, c, d, e, f) Al-Mn, Al-Mn-Zr, Al-Mn-Zr-Si, Al-Mn-Zr-Fe, and Al-Mn-Zr-Si-Fe alloys after the whole two-step annealing procedure ($Z = 8$).

surface as well as in the middle of the sheet. Figure 7 shows the corresponding grain structure at the surface of the sheets. The binary alloy (Fig. 7a) was selected as a representative of the cold rolled microstructure. The micrographs of other alloys in this condition are very similar. Figures 7b,c,d,e,f present the grain structure after the whole two-step annealing procedure ($Z = 8$). It can be clearly seen that only the Al-Mn-Zr alloy (Fig. 7c) remained unrecrystallized, exhibiting after annealing a similar microstructure as the cold-rolled binary alloy (Fig. 7a). All other alloys (Fig. 7b,d,e,f) show a (partially) recrystallized grain structure.

4. Discussion

The Mn-containing second phase particles can either stimulate or impede grain growth during ther-

momechanical treatment. Coarse particles ($> 2\,\mu m$) stimulate recrystallization by Particle Stimulated Nucleation (PSN); smaller particles ($< 0.5\,\mu m$) impede the grain growth by exerting a dragging force on grain boundaries (Zener drag). In the case of the studied materials with Zr addition, the Zener drag was exerted by two kinds of secondary particles – Mn--bearing phases (Al_6Mn, $Al_6(Fe,Mn)$, $Al_{15}Mn_2Si_3$ or α-$Al_{12}(Mn,Fe)_3Si$) and Zr-bearing Al_3Zr phase. In our study we used metallographic light microscope, which has a limiting resolution about 400 nm, and so we observed only relatively coarser Mn-bearing dispersoids. Finer Mn-bearing particles (< 400 nm), as well as very fine Al_3Zr dispersoids thus do not contribute to the particle density presented in Fig. 5. To include them in the study, a transmission electron microscope (TEM) or field emission gun scanning electron microscope (FEG SEM) would be necessary. However, even if we do not know the density of these finer particles, we can follow their influence in aggregate with coarser Mn-bearing dispersoids indirectly on the grain structure of the alloys indicating the recrystallization resistance.

If we compare the results of LM observation of the distribution of the particles and the grain structure at the end of the whole annealing procedure (Figs. 6, 7), there are important differences between the alloys. As the Al-Mn-Zr-Si and Al-Mn-Zr-Si-Fe alloys (Fig. 6b,d) contain a high number of coarse Particles Stimulating Recrystallization (PSN), numerous recrystallized grains 10 to 100 μm in size are present in the whole volume of the sheet (Fig. 7d,f). On the other hand, in the Al-Mn alloy there were no coarse Al_6Mn particles to stimulate recrystallization by PSN, neither fine Mn-bearing nor Al_3Zr dispersoid to inhibit the grain growth. In consequence, the recrystallized grains are coarse, pancake shaped along the rolling direction (Fig. 7b). The Al-Mn-Zr--Fe alloy shows fine recrystallized grains at the surface of the sheet (Fig. 7e) formed after PSN by coarse particles (Fig. 6c – surface), in the deeper regions, where these coarse particles are not present (Fig. 6c – middle) there are pancake shaped recrystallized grains (Fig. 7e). The only alloy, which remained unrecrystallized, was the ternary Al-Mn-Zr one (Fig. 7c), showing a uniform density of Al_6Mn particles (Fig. 6a), which are not sufficiently coarse to provoke PSN. Furthermore, at the same time it contains most probably the highest density of very fine Al_3Zr particles being under the resolution limit of light microscopy. The best results for the Al-Mn-Zr alloy in the hardness decrease (Fig. 4a) can also be attributed to the fine dispersion of Al_3Zr particles retaining the cold rolled microstructure, which is only recovered. Our results thus suggest that the additions of Fe and/or Si to the ternary Al-Mn-Zr alloy have rather negative effect and so their amount in the commercial materials should be reduced. This is in contradiction to the results in the literature [3, 15, 17, 18]. The explanation of the differences could be in the fact that the precipitation behaviour of the Mn- and Zr-bearing particles very likely strongly depends on the content of main alloying elements. So even if there was a positive effect of Si and also Fe on the Al_3Zr dispersoid formation reported, it was on different Al-Zr compositions. Nakamura et al. [15] used Al-0.6wt.%Zr alloy, Sato et al. [17] studied alloys containing 0.23 to 0.61 wt.% Zr, and the compositions of the alloys studied by Belov et al. [18] ranged from 0.5 to 1.0 wt.% Zr. The commercial purity alloy containing 0.17 wt.% Zr investigated by Westengen et al. [3] is closer to our alloys, but it does not contain any Mn.

On the other hand, Jia et al. [5, 16], Li and Arnberg [13], Tangen et al. [19] or Forbord et al. [20] studied Al-1wt.%Mn alloys which were close to our composition also in terms of other additions, i.e. Zr, Si and Fe. Jia et al. [16] concluded that a two-step precipitation annealing had a positive effect on the recrystallization resistance of a DC cast Al-1Mn-0.15Zr (wt.%) alloy, namely when the first stage of the annealing was at 250 ℃. We used a similar two-step annealing with the same temperature levels (250 and 450 ℃), but with shorter soaking periods 10 and 15 hours at the corresponding temperatures, respectively, in comparison with 48 and 60 h in the Ref. [16]. In our case, the two-step annealing was only slightly better, yielding a comparable density of the particles at the surface and mostly higher in the middle of the sheets (Fig. 5b), and lower decrease in the particle density (Fig. 5c). The recrystallization resistance of the materials subjected to one- and two-step annealing was the same. Jia et al. [5] reported lower recrystallization resistance of a homogenized Al-1Mn-0.15Zr-0.15Si-0.21Fe (wt.%) alloy in comparison with a corresponding ternary alloy without Si and Fe. This is in agreement with our results showing rather negative effect of Si and Fe. But if the same alloy was unhomogenized, it showed a fair recrystallization resistance similar to that of the homogenized and unhomogenized ternary variant [5]. The effect of Si and Fe on the recrystallization resistance of Al-Mn alloys should therefore be investigated further. Perhaps a twin roll-cast microstructure, exhibiting a higher density of finer dispersoids, could give different results.

5. Conclusions

1. The density of precipitates in all five alloys after one- and two-step annealing was higher in the middle of the 2 mm sheets than in the surface regions. Coarse primary phases formed in the alloys Al-Mn-Zr-Fe, Al--Mn-Zr-Si and Al-Mn-Zr-Si-Fe. Higher amount of

these coarse particles was found close to the surface of the sheets than in the middle.

2. The type of the annealing (one-step vs. two-step) did not influence the evolution of hardness and electrical conductivity – the differences were only very small. Either the microstructure of the alloys was very similar. On the other hand it can be concluded that in the majority of cases the two-step annealing procedure led to the same or lower decrease of the particle density during annealing.

3. Small equiaxial grains were formed in the whole cross section of the sheets of the alloys with Si addition during annealing. It seems that Si leads to the formation of a higher number of recrystallization nuclei by means of PSN. Except Al-Mn-Zr, the alloys without Si (Al-Mn and Al-Mn-Zr-Fe) showed coarse pancake shaped grains in the surface regions of the sheets. The microstructure in the middle of the sheets remained cold-worked.

4. After annealing, the Al-Mn-Zr alloy showed the highest hardness. Only in this alloy a cold-worked microstructure with elongated grains and shear bands persisted in the whole cross section of the sheet after the entire one- or two-step annealing procedures. All other alloys in the same condition were (partially) recrystallized. It follows that the Si and/or Fe additions degrade the recrystallization resistance of the Al-Mn alloy with Zr addition. Therefore, their amount should be reduced in commercial alloys where recrystallization resistance is required.

Acknowledgements

Financial support from the Czech Ministry of Education, Youth and Sports (projects MSM6840770021 and 1M0566) is gratefully acknowledged.

References

[1] KAWAHARA, A.—NIIKURA, A.—DOKO, T.: Furukawa Review, *24*, 2003, p. 81.
[2] ROYSET, A.—RYUM, N.: International Materials Reviews, *50*, 2005, p. 19.
[3] WESTENGEN, H.—REISO, O.—AURAN, L.: Aluminium, *12*, 1980, p. 768.
[4] ROBSON, J. D.—PRANGNELL, P. B.: Acta Materialia, *49*, 2001, p. 599.
[5] JIA, Z.—HUA, G.—FORBORD, B.—SOLBERG, J. K.: Materials Science and Engineering, *A444*, 2007, p. 284.
[6] BIDULSKÁ, J.—BIDULSKÝ, J.—CENIGA, L.—KVAČKAJ, T.—CABIBBO, M.—EVANGELISTA, E.: Kovove Mater., *46*, 2008, p. 151.
[7] IZUMI, O.—OELSCHLE, D.: Scripta Metallurgica, *3*, 1969, p. 619.
[8] NES, E.: Acta Metallurgica, *20*, 1972, p. 499.
[9] ZEDALIS, M. S.—FINE, M. E.: Metallurgical Transactions A, *17*, 1986, p. 2187.
[10] KOLBY, P.—SIGLI, C.—SIMENSEN, C. J.: In: Proc. of 4th International Conference on Aluminium Alloys (ICAA4). Eds.: Sanders, T. H., Starke, E. A. Atlanta, USA, Georgia Institute of Technology 1994, p. 508.
[11] DE HAAN, P. C. M.—VAN RIJKOM, J.—SØNTGERATH, J. A. H.: In: Proc. ICAA5, Materials Science Forum, *217–222*, 1996, p. 765.
[12] ROBSON, J. D.: Materials Science Engineering, *A338*, 2002, p. 219.
[13] LI, Y. J.—ARNBERG, L.: Acta Materialia, *51*, 2003, p. 3415.
[14] CIESLAR, M.—SLÁMOVÁ, M.—UHLÍŘ, J.—COUPEAU, C.—BONNEVILLE, J.: Kovove Mater., *45*, 2007, p. 91.
[15] NAKAMURA, F.—HIROSAWA, S.—SATO, T.: In: Proc. of 9th International Conference on Aluminium Alloys (ICAA9). Eds.: Nie, J. F., Morton, A. J., Muddle, B. C. North Melbourne, Institute of Materials Engineering Australasia Ltd. 2004, p. 582.
[16] JIA, Z.—HUA, G.—FORBORD, B.—SOLBERG, J. K.: Materials Science and Engineering, *A483–484*, 2008, p. 195.
[17] SATO, T.—KAMIO, A.—LORIMER, W.: In: Proc. ICAA5, Materials Science Forum, *217–222*, 1996, p. 895.
[18] BELOV, N. A.—ALABIN, A. N.—ISTOMIN-KASTROVSKIY, V. V.: In: Proc. of 9th International Conference on Aluminium Alloys (ICAA9). Eds.: Nie, J. F., Morton, A. J., Muddle, B. C. North Melbourne, Institute of Materials Engineering Australasia Ltd. 2004, p. 1270.
[19] TANGEN, S.—BJERKAAS, H.—FURU, T.—NES, E.: ibid., p. 1229.
[20] FORBORD, B.—HALLEM, H.—MARTHINSEN, K.: ibid., p. 1263.